Open Ceramics 7 (2021) 100161

Contents lists available at ScienceDirect

Open Ceramics

journal homepage: www.sciencedirect.com/journal/open-ceramics

Why freeze-casting brings different phase composition of calcium phosphates?

L. Pejchalová *, J. Roleček, D. Salamon

Central European Institute of Technology, Brno University of Technology, Brno, Czech Republic

ARTICLE INFO

Keywords:
Freeze-casting
Bioceramics
Calcium phosphates
Phase transformation
Porosity
Scaffolds

ABSTRACT

The impact of freeze-casting on the porosity, pore distribution, and phase composition was studied and compared with conventional shaping techniques. A bimodal pore size distribution was observed in freeze-cast + freeze-dried samples, in contrast to the unimodal one in freeze-cast + air-dried and conventionally prepared samples. The densification of freeze-cast + freeze-dried samples started at about 50 °C higher than their conventional counterparts (~870 °C vs. 920 °C). Diffusion seems to be a key parameter for the phase transformation of HAP into β-TCP during sintering. The residual HAP content in the sintered samples was influenced by used freezing rate and varied from 4% to 30% (unimodal samples), and from 7% to 16% (bimodal samples). Although further experiments must be carried out, our results showed that the freeze-casting parameters affect the resulting porosity and phase composition regardless of whether the freeze-drying or air-drying was used afterward.

1. Introduction

The development of highly porous ceramic scaffolds is a very important task in the field of bone tissue engineering and regenerative medicine. Calcium phosphate ceramics are commonly used as a feedstock material for bone scaffolds due to their chemical suitability, which is given by their natural presence in the human bones [1]. This determines their outstanding biological properties such as bioactivity, biocompatibility and biodegradability [1,2]. The biocompatibility and bioactivity are closely related to resorption of calcium phosphate ceramics in body environment [2]. The main representative of biocompatible and bioactive calcium phosphates is hydroxyapatite [1]. The solubility and degradation rate of scaffolds in the body fluids are very important characteristics influencing the bone remodelling process, driven by the resorption of calcium and phosphate ions released from the scaffold [2]. In the case of biodegradable and soluble calcium phosphates, both forms of tricalcium phosphate – alpha and beta – are most commonly used [1]. The group of calcium phosphate ceramics includes many compounds varying in the chemical formula, Ca/P ratio, solubility values, related degradation rates, etc. These differences can significantly influence regenerative processes in human bones [2,3].

This work is focused mainly on two types of calcium phosphates – hydroxyapatite (HAP) and beta-tricalcium phosphate (β-TCP), which differ in chemical composition, solubility, and degradation rate [3]. Both, HAP and β-TCP, are commonly used in regenerative medicine in several forms, such as granules, cements, coatings or porous scaffolds [4,5]. The phase transformation of calcium phosphates occurs mainly during the heat treatment, e.g. calcination or sintering, and is influenced mostly by physico-chemical parameters [6]. Thermal transformation of HAP into β-TCP starts at temperatures ranging from 600 °C to 800 °C, when the dehydroxylation of HAP appears and is partially transformed into β-TCP. The complete phase transformation of HAP requires higher temperatures, around 1100 °C [3], and the resulting β-TCP remains stable up to 1200 °C [7]. At this temperature pressure-less sintering of calcium phosphates is generally performed, thus the process of phase transformation takes place in parallel with the densification of the material. For both, phase transformation and sintering, the solid-state diffusion is required. Physical parameters of calcium phosphate ceramics, such as grain size and morphology, specific surface area, pore distribution and green body density influence the kinetics of sintering as well as the phase transformation [7]. Furthermore, previous studies [7,8] have shown that phase transformation of calcium phosphates, mainly HAP and β-TCP, is affected not only by the above mentioned parameters, but also by the used shaping techniques and microstructural design. For example, Itatani et al. [9] presented a study where starting powder, composed of HAP and β-TCP, was uniaxially pressed and sintered at 1070 °C for 5 h. The phase composition of the resulting sintered compacts was composed completely of β-TCP. The effect of cold isostatic

* Corresponding author.
E-mail address: Lucie.Pejchalova@ceitec.vutbr.cz (L. Pejchalová).

https://doi.org/10.1016/j.oceram.2021.100161
Received 29 January 2021; Received in revised form 2 July 2021; Accepted 6 July 2021
Available online 8 July 2021

pressing (200 MPa), and various sintering temperatures (1000–1300 °C) applied on nanocrystalline hydroxyapatite (with Ca/P ratio of 1.67) was presented by Ramesh et al. [10]. Surprisingly, no secondary phases were indicated by XRD analysis, and hydroxyapatite phase remained stable during sintering.

As aforementioned, starting chemical composition of calcium phosphates plays a crucial role in the phase transformation process. Changes in Ca/P ratio, ionic substitutions in the crystal structure, calcium deficiency or metastable phases influence chemical reaction pathways during sintering and thus the final phase composition of calcium phosphates [3,7]. In particular, the addition of alkali cations (lithium, sodium or potassium), or their substitution for calcium cation in hydroxyapatite, creates OH^- vacancies in the lattice. This procedure may enhance solid-state diffusion during sintering and contribute to achieving a better densification and phase transformation of HAP into β-TCP [7]. Other several factors, such as sintering parameters (atmosphere, dwell, sintering method, temperature), amount of water/-moisture, and pre-treatments (washing, calcination, using additives) can affect both, sintering and phase transformation. Hence, it is difficult to precisely describe the mechanism of phase transformation of calcium phosphate-based materials or to determine the exact factor, which influences the process of phase transitions [6,7].

Besides, the microstructure and porosity of calcium phosphate scaffolds play a significant role regarding also the bone regeneration process [3]. The ideal processing technique for scaffold preparation should produce mechanically stable structures with controlled pore size, shape and distribution, which is important for the diffusion of nutrients throughout the scaffold and bone tissue ingrowth. However, the mechanical stability of scaffolds is highly limited by introduced porosity transitions [11,12]. Freeze-casting, also known as ice-templating, is a simple and versatile shaping method that allows the production of highly porous ceramics with sufficient mechanical stability and controlled interconnected porosity [13]. During the freeze-casting, a solvent in a ceramic suspension (most commonly water) is solidified and the inner structure is formed via directional growth of solvent crystals. Subsequent step of the process, freeze-drying (lyophilization), allows to sublimate the solvent crystals without damaging the microstructure, which is a replica of the solvent crystals [12]. The resulting microstructure can be modified by manipulating the crystallization behaviour of the solvent, using additives and cryoprotectants into the starting ceramic suspension, or by changing the freezing step parameters (e.g. freezing front velocity) [14]. The freeze-casting has been reported by many studies to be a suitable method for preparation of hierarchically structured bioceramics [12–15]. Study presented by Seifert et al. [16], has shown that freeze-casting can be successfully applied on a wide variety of calcium phosphate materials, and their final phase composition can be modified by addition of another phase or compound [17]. Furthermore, lamellar structures with the size of interlamellar spaces larger than 100 μm, can be inhabited by bone cell colonies and the used bioactive material can induce their proliferation and bone ingrowth [18,19].

In our previous study [20], we have shown the variability of freeze-casting for HAP/β-TCP scaffold preparation, but several differences in sintering behaviour and phase composition, compared to robocast scaffolds made from the same starting powder, were observed. So, the aim of this study is to further explore these differences and to prepare HAP/β-TCP scaffolds with wide range of porosities, using different shaping techniques and the same starting powder. Conventional shaping techniques (e.g. slip-casting, cold isostatic pressing) and freeze-casting with various freezing front velocities are used to prepare green bodies. Two different drying methods (freeze-drying and air-drying) are employed on the freeze-cast samples to provide additional information. Sintering of all samples is performed at the same temperature and the density, porosity, shrinkage, microstructure and phase composition are evaluated to understand the impact of freeze-casting process on sintering behaviour and phase transformation of calcium phosphates. The plausible reasons, why the freeze-casting process brings different phase compositions of calcium phosphate scaffolds are stated and discussed.

2. Materials and methods

2.1. Starting powders

Commercially available hydroxyapatite powder (purum p.a., $Ca_5(OH)(PO_4)_3 > 90\%$, Sigma-Aldrich) was used as a starting ceramic material. Before further use, the powder was calcined at 800 °C for 60 min in air atmosphere. Residual carbonates were removed during the calcination process and a starting biphasic calcium phosphate mixture, comprised of HAP and β-TCP, was formed. Both, raw and calcined powder were separately examined by X-ray diffractometry to determine their phase composition. The resulting biphasic mixture was used for the preparation of all the green bodies.

2.2. Green body preparation

Porous ceramic samples were prepared by freeze-casting of water-based HAP/β-TCP suspension. The same ceramic suspension was used to prepare slip-cast samples. Dry shaping technique, namely cold isostatic pressing, was utilized (using the same starting biphasic powder) to produce comparative samples. Sets of 12 samples were prepared using each fabrication method.

Since the number of variants is quite high, in order to provide a clear overview in the obtained results a schematic illustration of the green body preparation techniques and corresponding sample identifiers is presented in Fig. 1.

2.2.1. Starting suspension

The biphasic calcined powder was used for ceramic suspension preparation, with a solid loading of 15 vol%, according to the whole volume of suspension. A poly(vinyl alcohol) (1.3 vol% according to the whole volume; Mowiol® 10–98, Sigma-Aldrich) was used as an organic binder, and a carbonic acid polyelectrolyte (2.3 vol% according to the whole volume; Dolapix CE 64, Zschimmer&Schwartz) was used as a dispersant. Sucrose in the concentration of 3 wt%, according to the ceramic powder, was added to the suspension to modify the crystallization behaviour of growing ice crystals, to enhance resulting mechanical properties of freeze-cast samples.

2.2.2. Freeze-casting

The fabrication of porous calcium phosphate samples was performed using the freeze-casting method. A freeze-casting mould with embedded copper block in the bottom, was printed on a 3D printer from poly(lactic acid) – PLA (Plasty Mladeč). The inner diameter of the mould was 24.5 mm and the height 50 mm. Several freezing rates were facilitated using different cooling methods: cooling plate, fast cooling with liquid nitrogen and dipping a plastic Pasteur pipette with the suspension into a liquid nitrogen bath. A continuous decreasing of the cooling plate temperature allows to control the freezing rate and thus the lamellae formation and the interlamellar distances. Two different speeds of the cooling plate temperature decrease, as well as two different set ups for liquid nitrogen cooling, were chosen to achieve various freezing rates (see Table 1). After complete freezing, the samples were removed from the mould and placed in a freezer (−20 °C) before further processing, to equalize the temperature throughout their whole volume.

Two different drying procedures were used for freeze-cast samples after the freezing step, freeze-drying and air-drying. Freeze-drying, by sublimation of ice crystals, was conducted in a vacuum chamber at a pressure of ca. 10 Pa for 24 h with a gradual temperature increase up to 30 °C. This controlled procedure prevented a damage of the lamellar structure of freeze-cast bodies by ice melting or by reaching the sugar glass transition temperature. These freeze-dried samples were marked as

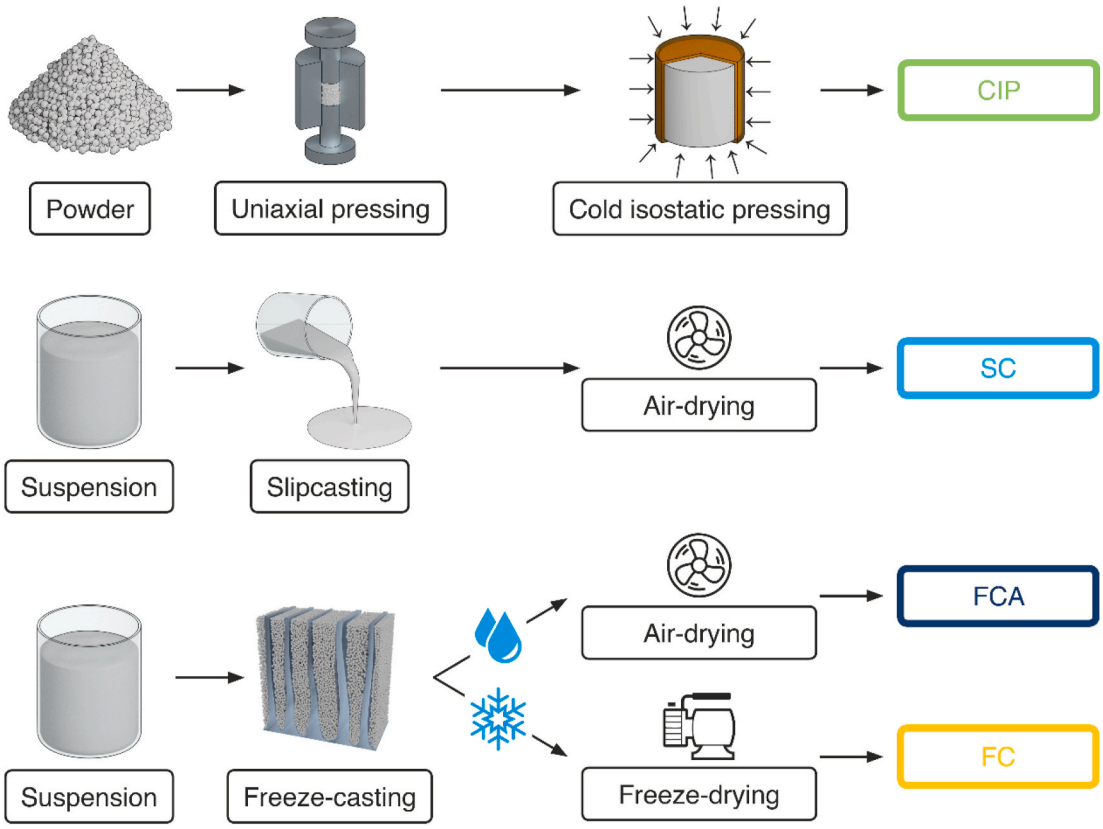

Fig. 1. Schematic illustration of green body preparation techniques used in this study and corresponding sample identifiers. (For interpretation of the references to colour in this figure legend, the reader is referred to the Web version of this article.)

Table 1
Average freezing front velocities assigned to the type of freezing method and corresponding sample identifiers.

Freezing method	Sample identifier	Average freezing front velocity [μm/s]
Cooling plate	FC1; FCA1	3.4 ± 0.3
	FC2; FCA2	5.5 ± 0.2
Liquid nitrogen (freezing bath)	FC3; FCA3	12.7 ± 0.5
	FC4; FCA4	25.8 ± 1.2
Liquid nitrogen (dipping)	FC5; FCA5	~1000

FC1-FC5, where 1–5 stands for the freezing rate applied, as described in Table 1.

A second set of freeze-cast samples was thawed to obtain dense samples. Samples were taken out of the freezing mould, placed into a polyethylene mould, and let to thaw. During thawing, the ice crystals melted, and the lamellar structure collapsed. Thawed suspensions were let to dry at ambient temperature. These samples are denoted as FCA1-5, where 1–5 stands for the freezing rate applied, as described in Table 1.

2.2.3. Conventional shaping techniques

Two conventional shaping techniques, cold isostatic pressing and slip-casting, were used for the preparation of comparative samples. The same ceramic suspension, as for the freeze-casting, was used for slip-casting technique. A given amount of mixed and deaerated suspension was poured into a polyethylene mould and let to dry at ambient temperature. These types of samples are marked as SC (Fig. 1).

For cold isostatic pressing, the green pellets were prepared using semi-automatic uniaxial press BSML 21 – MT 20 (Brio Hranice). Approximately 0.5 g of calcined powder was poured into a stainless-steel die (inner diameter of 16 mm) and pressed at 10 MPa. Prepared green pellets were placed into an elastic cover, the inner space was evacuated and the cover sealed. A set of sealed pellets was placed in an isostatic press P/O/WEBER (Laborpresstechnik), pressed at 700 MPa, and taken out of the protective elastic cover (denoted as CIP, see Fig. 1).

2.2.4. Sintering

Sintering of all prepared green bodies was performed at 1200 °C for 120 min in air atmosphere. The heating rate was set to 2 °C/min up to 600 °C and then 5 °C/min up to 1200 °C. The cooling rate was set to 5 °C/min down to 700 °C, then the furnace was turned off and samples were let to cool down to ambient temperature.

2.3. Characterization

2.3.1. Scanning electron microscopy

Micrographs of obtained microstructures were taken using a High-Resolution Scanning Electron Microscope Verios 460L (FEI). Images were taken from the sample's surface by scanning secondary and backscattered electrons, at low voltage (5 kV). The microstructural characteristics were examined, and the linear intercept method was used for grain size determination (EN 13383-1) [21].

2.3.2. Porosity

Relative porosity of freeze-cast porous samples was calculated from the sample weight and dimensions after sintering. Density measurements, used for dense samples, were performed using the Archimedes method (EN 623-2) [22].

To determine the intergranular pore size distribution, a mercury intrusion porosimetry measurements were performed using a porosimeter Pascal440 (Thermo Fischer Scientific), with a measuring pressure set to 330 MPa.

2.3.3. X-ray diffractometry

X-ray diffraction (XRD) analyses for phase composition determination were performed using the high-resolution diffractometer with Cu anode Rigaku SmartLab 3 kW (Rigaku). The XRD was operated at 40 kV voltage and 30 mA current in Bragg-Brentano measurement mode. The XRD spectra were taken from powder or surface of bulk samples. Determination of the hydroxyapatite and β-TCP amount from the XRD spectra was obtained using the simple height law for the I_{100} peaks. Therefore, the percentage of hydroxyapatite (HAP) was determined by the following formula [23]:

$$\text{HAP } [\%] = \frac{I_{100}(\text{HAP})}{I_{100}(\text{HAP}) + I_{100}(\text{TCP})} \cdot 100$$

2.3.4. Dilatometry

Prism-shaped samples (ca. 1.0 × 3.0 × 4.5 mm) were prepared from several types of freeze-cast, slip-cast and CIP green bodies. The samples were sintered in a dilatometer L70/1700 (Linseis) at 1200 °C for 120 min in air atmosphere. The heating rate was set at 2 °C/min up to 600 °C and 5 °C/min up to 1200 °C. The cooling rate was set at 10 °C/min. Dilatometric curves were recalculated backwards according to Maca et al. [24]. Relative densities of sintered samples were measured using the Archimedes method.

3. Results

3.1. Microstructure

The SEM micrographs of green bodies (Fig. 2) were taken to observe the influence of different shaping techniques on resulting microstructure, as well as the influence of applied freezing front velocity on interlamellar distances of freeze-cast + freeze-dried samples before sintering. The microstructure of green body CIP samples (Fig. 2a) contain quite a high amount of large square agglomerates, despite the fact that a pressure of 700 MPa was applied. Micrographs of similarly fabricated samples SC and FCA5, depicted in Fig. 2b and c, respectively, show the impact of the freezing on the resulting microstructure. It can be seen that the green body microstructure of the FCA5 samples (Fig. 2c), which is composed of fine agglomerates, differs significantly from microstructure of the slip-cast samples (Fig. 2b) in which the microstructure is much finer and ceramic particles are distributed more homogenously.

SEM micrographs of FC2 and FC5 green bodies can be seen in Fig. 2d and e, where is apparent that homogenously distributed tiny lamellae and interlamellar spaces were also formed in the FC5 samples, despite the extremely fast freezing rate (Table 1). However, there is an enormous difference in interlamellar spaces between FC2 and FC5 samples, which is in agreement with measurements of interlamellar distances, summarized in Table 2.

Differences in grain sizes of various sintered samples (1200 °C/120 min) are depicted in Fig. 3. There are no significant differences in grain sizes of samples prepared by conventional techniques (CIP, SC) and freeze-cast + air-dried samples (FCA5), see Fig. 3a and b vs. Fig. 3c. These observations were also confirmed by the results of grain size measurements using the linear intercept method. For CIP samples the grain size was 2.73 ± 0.39 μm, for SC samples 2.38 ± 0.25 μm, and for FCA5 samples 2.41 ± 0.26 μm.

Interestingly, the microstructure of lamellae in the freeze-cast +

Table 2
Average values of interlamellar spaces, relative porosities and HAP content of freeze-cast + freeze-dried (FC) samples after sintering at 1200 °C/120 min.

Sample identifier	Interlamellar spaces [μm]	Relative porosity [%]	HAP content [%]
FC1	108.2 ± 18.7	66.7 ± 0.6	16
FC2	64.1 ± 10.7	70.7 ± 0.1	16
FC3	45.0 ± 7.6	72.3 ± 0.0	13
FC4	19.9 ± 3.6	72.6 ± 0.4	8
FC5	~1	66.9 ± 0.3	7

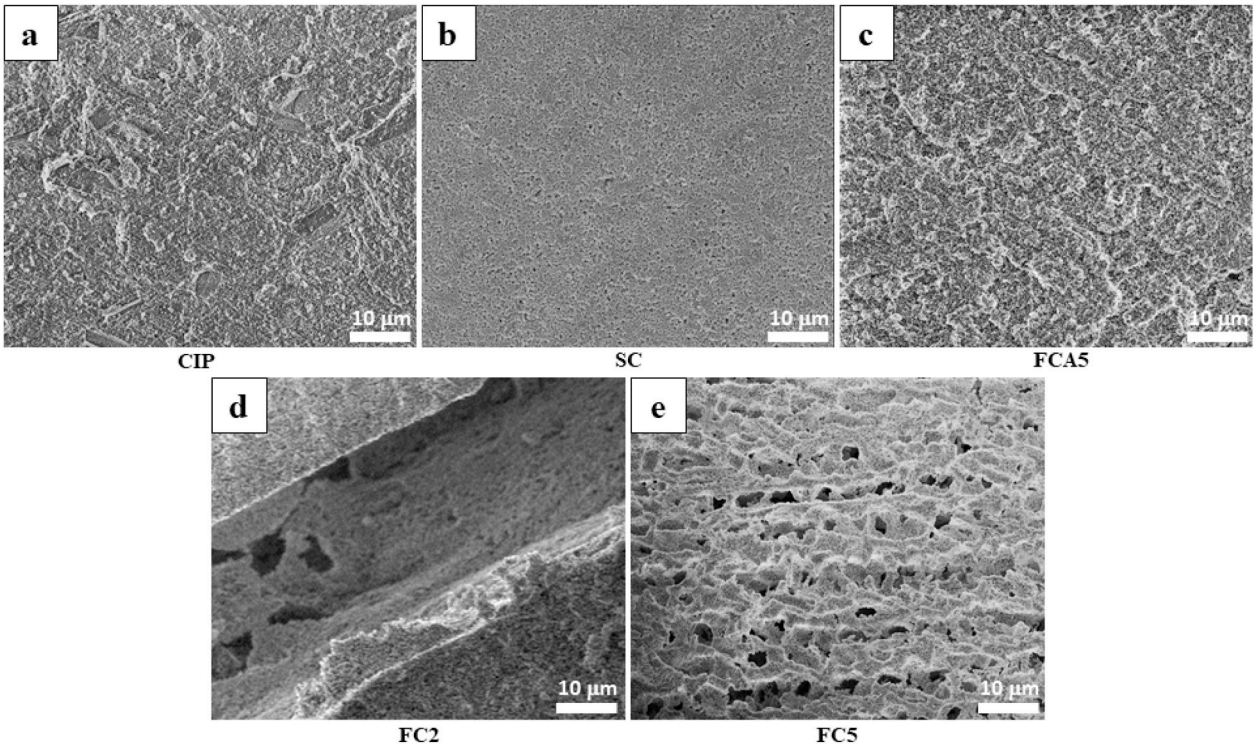

Fig. 2. SEM micrographs of green body samples; a – isostatically pressed (CIP), b – slip-cast (SC), c –freeze-cast + air-dried (FCA5), d – freeze-cast + freeze-dried (FC2), e – freeze-cast + freeze-dried (FC5).

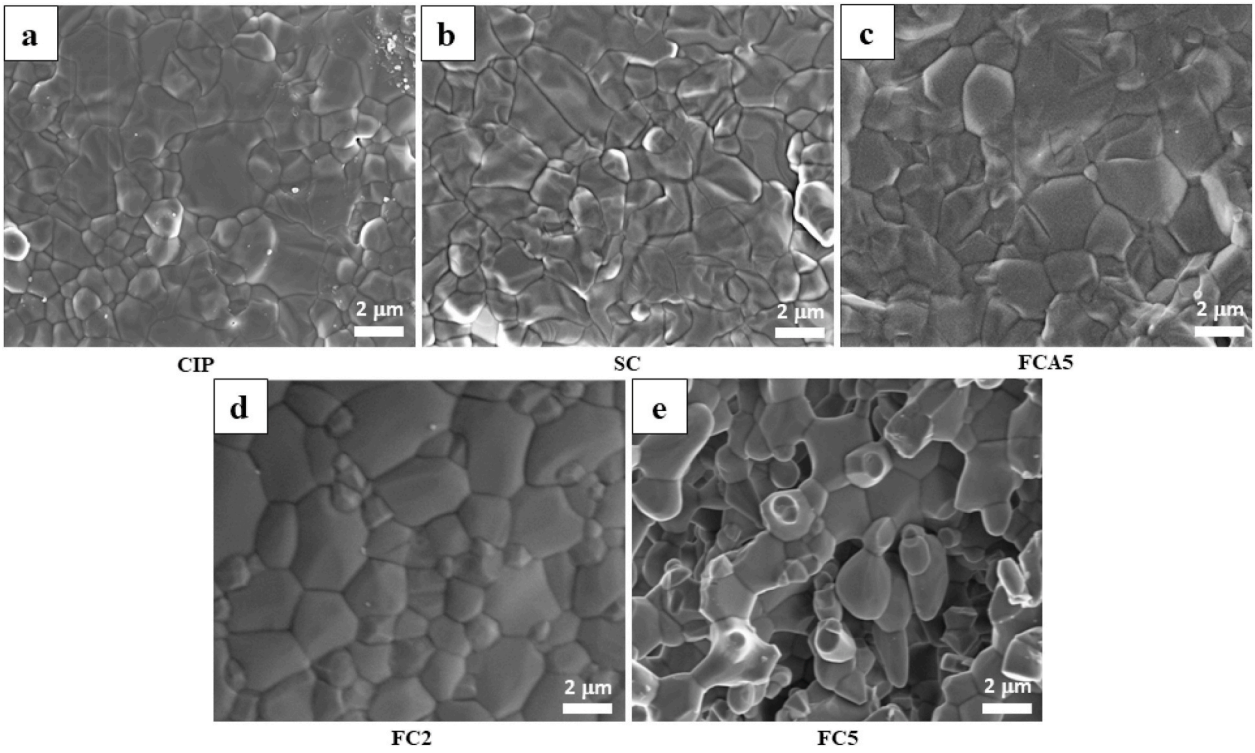

Fig. 3. SEM micrographs of sintered samples; a – isostatically pressed (CIP), b – slip-cast (SC), c – freeze-cast + air-dried (FCA5), d – freeze-cast + freeze-dried (FC2), e – freeze-cast + freeze-dried (FC5).

freeze-dried samples (FC2), see Fig. 3d, is quite similar to the aforementioned samples. This suggest that lamellae are almost fully dense and the porosity is formed mainly by the interlamellar spaces. The SEM micrographs revealed that the FC5 samples are quite porous on microscale, despite the fact that their total porosity is lower, compared to FC2-4 samples (see Table 2).

3.2. Porosity

Total porosity and interlamellar spaces measurements were performed on porous freeze-cast + freeze-dried samples sintered at 1200 °C for 120 min, and the results, along with HAP content from XRD analyses, are summarized in Table 2.

The highest relative porosity values were achieved by freeze-casting using the liquid nitrogen for cooling (FC3 and FC4 samples). On the other hand, the lowest porosity values (66.7 ± 0.6% and 66.9 ± 0.3%) were observed in the samples frozen on the cooling plate with the slowest temperature decrease (FC1) and in the samples prepared by the fastest cooling method by dipping in a liquid nitrogen (FC5), respectively.

Relative densities of green bodies and sintered samples, prepared by freeze-casting followed by thawing and air-drying (FCA1-5), as well as comparative slip-cast (SC) and isostatically pressed samples (CIP) are shown in Table 3.

The green body densities of FCA samples increase with increasing freezing rate, reaching the maximum value of 55.4 ± 0.7%, for samples dipped in the liquid nitrogen. However, the relative densities of sintered samples do not show exactly the same trend and the maximum relative density of 98.2 ± 0.8% was reached in samples frozen by the second fastest cooling rate (FCA4), but it is necessary to consider that the relative densities of the FCA5 samples have relatively large variance (95.3 ± 4.3%).

Slip-cast samples, which preparation route was the same as in the case of FCA samples, except for the freezing step, had a relative green density 46.6 ± 0.6%, which is between FCA2 and FCA3 samples, but the relative density 98.9 ± 0.6% of sintered SC samples was superior even to FCA4 samples. As expected, both, the highest green and sintered relative densities, were observed in the isostatically pressed samples with values of 63.9 ± 0.9% and 99.3 ± 0.4%, respectively.

Table 3
Average values of relative densities of green and sintered samples, along with and HAP content in sintered samples (1200 °C/120 min) prepared by isostatic pressing (CIP), slip-casting (SC) and freeze-casting + air-drying (FCA).

Sample identifier	Green body relative density [%]	Sintered relative density [%]	HAP content [%]
CIP	63.9 ± 0.9	99.3 ± 0.4	4
SC	53.4 ± 0.6	98.9 ± 0.6	20
FCA1	38.9 ± 0.3	89.1 ± 0.6	25
FCA2	44.3 ± 0.4	97.2 ± 0.4	24
FCA3	49.5 ± 0.3	95.2 ± 0.2	30
FCA4	52.8 ± 0.5	98.2 ± 0.8	21
FCA5	55.4 ± 0.7	95.3 ± 4.3	27

Mercury porosimetry measurements were performed on various green bodies prepared by different techniques, to compare their pore size distributions. Selected porosimetry results can be seen in Fig. 4.

Based on the pore size distribution, the samples can be divided in two groups: unimodal porosity samples (with pores between grains only), and bimodal porosity samples, containing porosity between grains as well as interlamellar porosity. Bimodal pore size distribution was observed in all freeze-cast + freeze-dried samples (FC1-5), despite an extremely fast freezing rate was used to freeze the FC5 samples. The mercury porosimetry measurement of the samples FC2 was not fully completed because interlamellar spaces in this sample were about 65 μm (see Table 2), and such big pores (interlamellar spaces) are out of the measurement range of the used porosimeter.

A unimodal pore size distribution was only observed in freeze-cast + air-dried samples, as well as in comparative slip-cast and isostatically pressed samples.

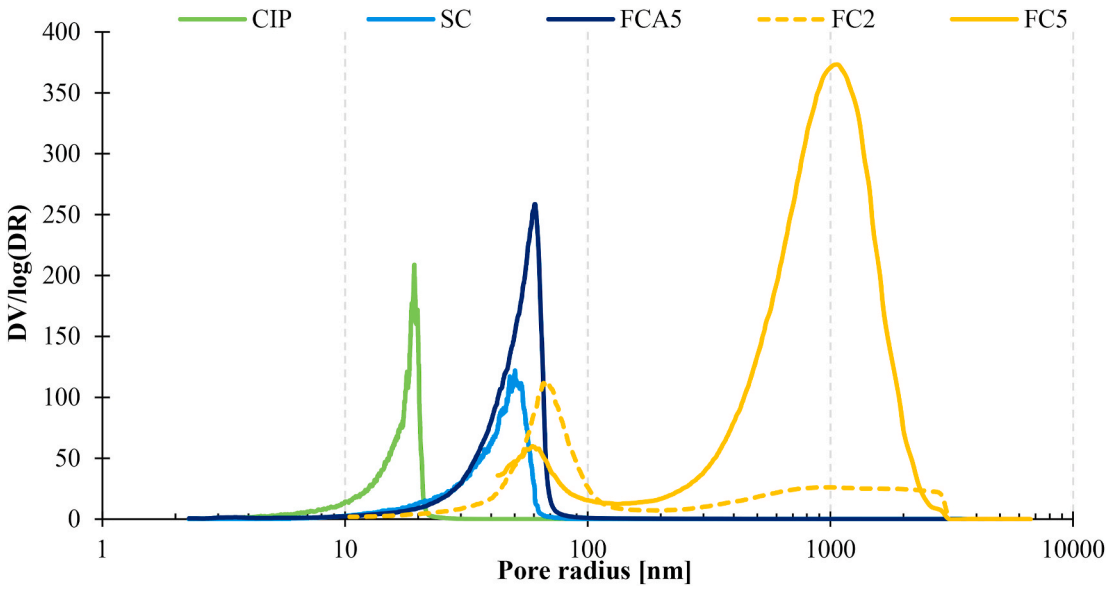

Fig. 4. A pore size distribution comparison of green body samples prepared by different techniques; isostatic pressing at 700 MPa (CIP), slip-casting (SC), freeze-casting + air-drying (FCA5) and freeze-casting + freeze-drying (FC2, FC5). (For interpretation of the references to colour in this figure legend, the reader is referred to the Web version of this article.)

3.3. Phase composition

XRD analyses were performed on original raw powder, calcined powder and sintered samples, to evaluate the effect of the processing method on the phase composition of sintered samples. The HAP content (~60%) in the calcined powder was calculated from obtained XRD patterns, that are depicted in Fig. 5, using height law for the I_{100} peaks. The results have shown that the amount of hydroxyapatite in the powder dropped by about 30% during calcination, when compared to the original starting powder, in which the declared amount of HAP was at least 90% (data taken from the datasheet supplied by the producer).

The residual HAP content in all freeze-cast + freeze-dried samples is given in Table 2, whereas the HAP content in all freeze-cast + air-dried samples is given in Table 3. The XRD patterns of selected samples are shown in Fig. 6. The phase composition of CIP samples is almost pure β-TCP, with just a few traces of the original HAP (~4%), which is the highest content of β-TCP among all the sintered samples. On the other hand, the highest amount of original HAP (~30%) was found in the freeze-cast + air-dried FCA3 samples, see Table 3.

3.4. Dilatometry

To clarify the differences in the sintering behaviour of samples prepared using different shaping techniques, dilatometry measurements were performed on freeze-cast + freeze-dried sample FC5, freeze-cast + air-dried sample FCA5, slip-cast and CIP samples. The obtained dilatometric curves are shown in Fig. 7. The inaccuracy in green body densities is given by the calculation method based on the densities after

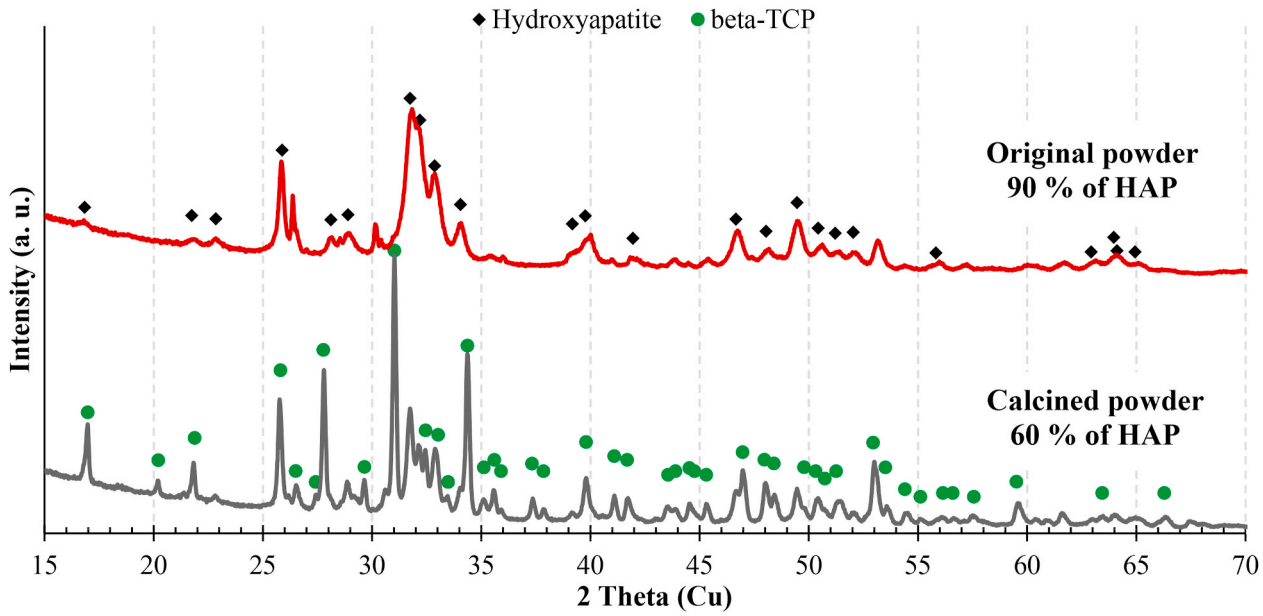

Fig. 5. XRD patterns of the original as received powder and the calcined powder (800 °C/60 min). HAP percentage in the calcined powder was counted using the height law for the I_{100} peaks. Main HAP and β-TCP peaks are identified with indicated symbols.

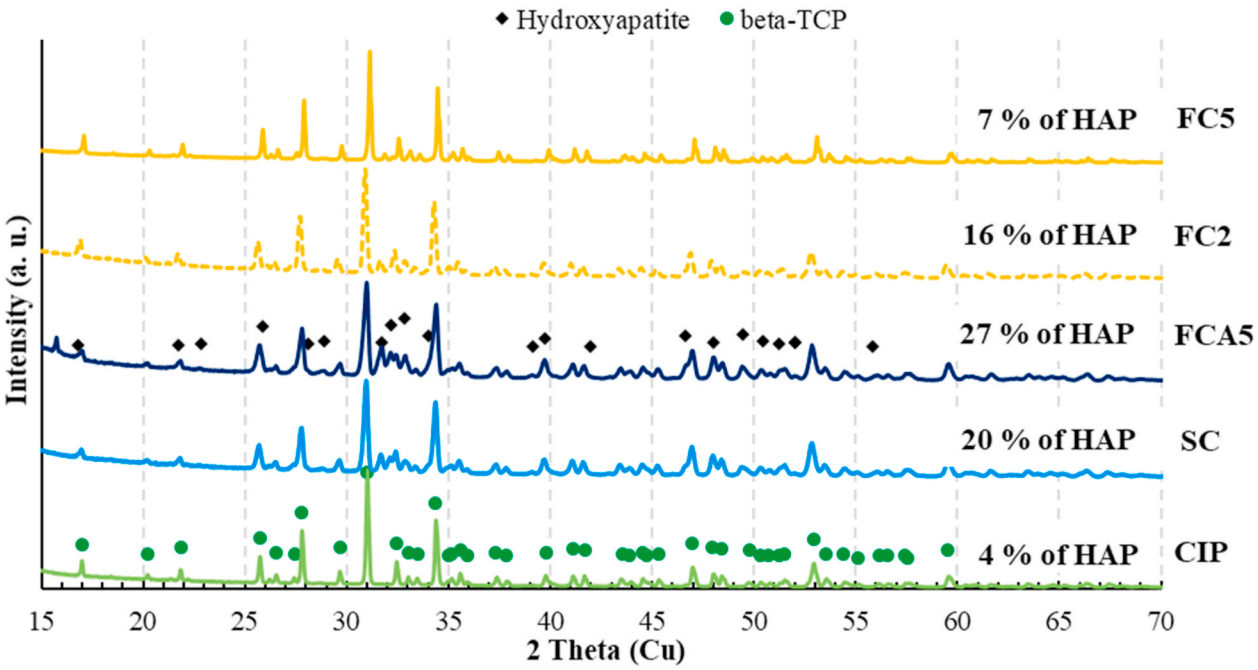

Fig. 6. *XRD analyses of sintered samples prepared by isostatic pressing at* 700 MPa *(CIP), slip-casting (SC), freeze-casting + air-dried (FCA5), and freeze-casting + freeze-dried (FC2 and FC5). The HAP percentage in the samples was counted using the height law for the I_{100} peaks. Main HAP and β-TCP peaks are identified with indicated symbols.*

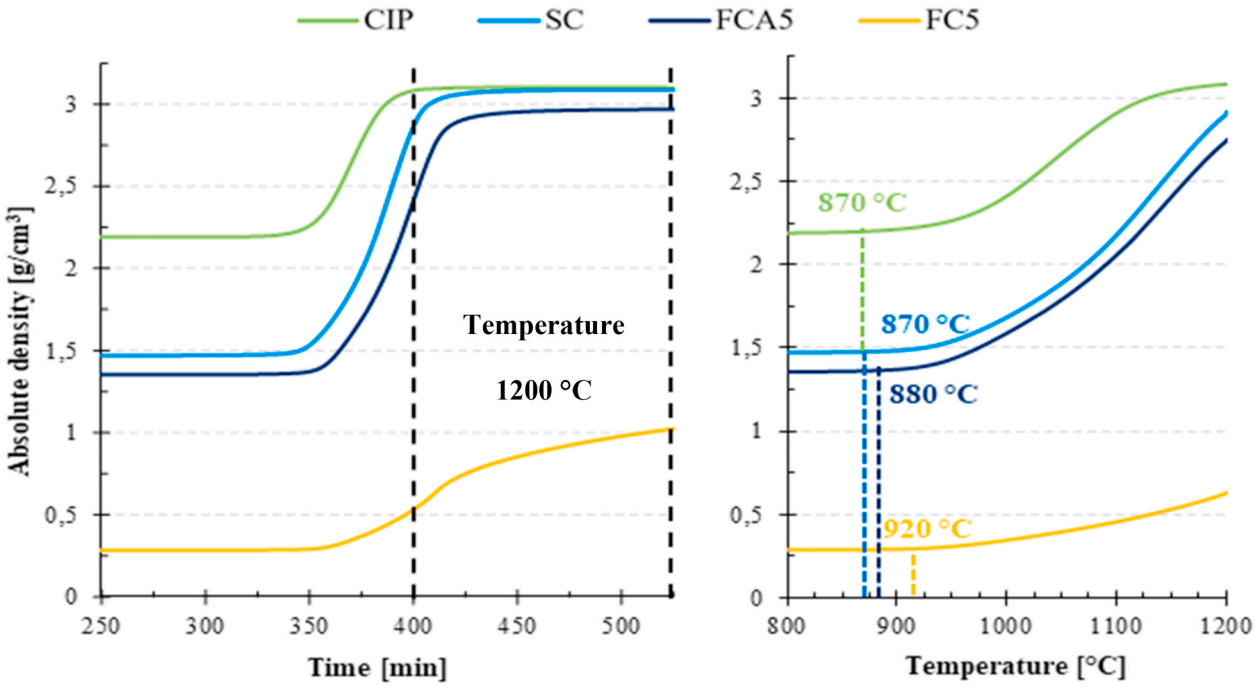

Fig. 7. Dilatometric curves of sintered samples prepared by isostatic pressing at 700 MPa (CIP), slip-casting (SC), freeze-casting + air-dried (FCA5), and freeze-casting + freeze-dried (FC5). Starting temperatures of densification are indicated for each sample.

sintering. The dilatometric analyses revealed that the sintering behaviour of slip-cast (SC) and freeze-cast + air-dried (FCA5) samples is unsurprisingly very similar, since the only difference in their preparation route is the implementation of the freezing step in the case of FCA5 samples. However, some differences in the densification process can be seen. The temperature when densification started was about 10 °C higher in the case of the freeze-cast sample (~870 °C vs. 880 °C) and the densification process of the CIP samples was finished even before reaching the final sintering temperature, without further changes in relative density during the dwell time.

The sintering behaviour of porous freeze-cast + freeze-dried FC5 samples differs among all the samples. The densification started later, compared to conventionally prepared samples, at about 920 °C, as in the case of FCA5, however the densification rate was very slow, and did not reach the final stage even after the 120 min' dwell at 1200 °C.

As the dilatometric measurements are based on a linear shrinkage of samples with more or less isotropic properties (in term of porosity and shrinkage), a simple comparison of FC samples with conventionally

prepared ones was not possible, as FC samples have anisotropic highly ordered lamellar microstructure. The only exceptions are FC5 samples frozen by dipping in liquid nitrogen, in which the microstructure is composed of extremely small uniformly distributed lamellae without directional orientation and some non-lamellar zones.

4. Discussion

The answer to the question 'why freeze-casting brings different phase compositions of calcium phosphates' can be found mainly in the green body microstructure. Freeze-casting, followed by lyophilisation and sintering, brings highly porous samples (total porosity of ~70%) with bimodal pore size distribution. Furthermore, different cooling methods and resulting freezing front velocities change the porosity and the size of interlamellar spaces. Increasing the freezing front velocity, the total porosity of sintered samples increases, while the size of interlamellar spaces decreases (see Table 2). These two trends fully correspond with the literature [14,15,25]. Bimodal pore distribution has been observed in the freeze-cast + freeze-dried green bodies, in contrast to the unimodal one present in all other samples (see the porosimetry curves in Fig. 4). If we compare intergranular porosities of FC2 and FC5 samples, we can see that the pores between ceramic particles differ very slightly in the size, but the volume of intergranular pores is clearly lower in the case of FC5samples. This is probably caused by high freezing front velocity (dipping the mould in liquid nitrogen), with a speed of about 1000 μm/s (compared to the freezing front velocity of FC2 samples with an average speed of 5.5 ± 0.2 μm/s). Low freezing front velocity led to higher compaction of ceramic particles and thus lowered the pore volume. This is also in a good correlation with total porosity results after sintering, as the relative porosity of FC5 samples is lower with value of 66.9 ± 0.3%, compared to 70.7 ± 0.1% of FC2 samples. It is also necessary to mention that the FC5 samples are exceptional, among the freeze-cast + freeze-dried samples, because they were prepared by non-directional freezing and thus, the resulting microstructure is fairly isotropic with very thin lamellae in many directions and some non-lamellar zones distributed throughout the whole samples. Interestingly, almost the same relative porosity after sintering was measured in the samples frozen by the slowest freezing front velocity (FC1), see Table 2. Although the explanation remains unknown, the ice crystals' slow growth (average freezing front velocity just 3.4 ± 0.3 μm/s) could have played a key role, giving the ceramic particles enough time to self-assemble in the emerging lamellae.

As aforementioned unimodal pore size distribution at the submicron level has been observed in conventionally prepared samples, as well as in the samples prepared by freeze-casting + air-drying (FCA5). A good correlation between green body densities and freezing rate can be observed in the case of FCA samples, where the higher the freezing rate, the higher is the resulting green body density (see Tables 1 and 3). These results suggest that lower freezing rates lead to higher internal pressures due to the ice crystals growth, promoting a higher occurrence of agglomerates and thus lower green body density.

FCA5 and SC samples, that share the same preparation route except for the freezing step in the case of FCA samples, are also comparable in terms of green body density and pore size. The main difference between them can be found in the volume of intergranular pores. A higher volume of pores is found in FCA5 samples, compared to SC samples (Fig. 4), due to the presence of agglomerates, which were also observed in the SEM micrographs (Fig. 2). Similar results were also obtained by Zheng et al. [26], in the study regarding the freeze-casting influence on the sintering behaviour of alumina. As well as in our presented study, they observed changes in green body and sintered densities, and sintering behaviour as well, derived from the shaping process. All these correlations, according to our presented work, also applies for calcium phosphate materials.

Cold isostatically pressed samples showed the highest values of green body relative density (~64%) as well as and relative density after sintering (~99%) among all the samples. In addition, CIP samples exhibited a very narrow pore size distribution (Fig. 4). Such results are not unexpected due to the very high applied pressure of 700 MPa.

The dilatometric analyses (Fig. 7) indicate that the sintering behaviour and densification process differ mainly among the conventionally prepared samples and samples where the freeze-casting was applied (FC and FCA). The dilatometric curve of CIP samples has shown that its densification started at ~870 °C and the sample was almost fully sintered even before reaching the sintering temperature of 1200 °C. Regarding the samples using the same ceramic suspension as feedstock also differences were observed. The densification of SC samples started at ~870 °C compared to ~880 °C and ~920 °C in the case of FCA5 and FC5 samples, respectively. The reason, why freeze-casting is shifting the start of the sintering to higher temperatures is still not clear however, the literature data [26] and the microstructural observation (Fig. 2) suggest that the main reason is the presence of ceramic agglomerates in freeze-cast samples.

The main part of the phase transformation of hydroxyapatite into β-TCP by dehydroxylation occurred during the sintering at 1200 °C. At this temperature, hydroxyapatite decomposed into β-TCP and this process is most probably driven by sufficient diffusion, which is necessary for the phase transformation. It has already been reported [27–29] that the dehydroxylation of HAP begins already at 630 °C and intensifies with increasing the temperature, resulting in β-TCP which becomes the major phase. As the dehydroxylation process in the starting powder can only take place up to the calcination temperature of 800 °C, it is not possible to achieve a complete transformation of HAP into β-TCP during the calcination. Thus, the starting powder is a biphasic mixture of 60% HAP and 40% β-TCP (see XRD spectra in Fig. 5), being hydroxyapatite the major phase. The diffusion in prepared samples should be the key parameter for the phase transformation of HAP into β-TCP during sintering. Therefore, we can state that the used shaping method and resulting microstructure, mainly total porosity and pore size distribution, influence the diffusion and thus final phase composition. As can be seen from obtained XRD spectra in Fig. 6, the content of residual hydroxyapatite after sintering varies among all samples. The lowest content, about 4% of hydroxyapatite, was observed in CIP samples. Such a low amount of residual hydroxyapatite was most probably caused by the high pressure applied to the starting powder, which was accompanied by redistribution of ceramic particles. Similar results, for starting biphasic mixture of HAP and β-TCP, were obtained by Itatani et al. [9] after uniaxial pressing and sintering at 1070 °C. According to several reviews [3,7,8], the sintering temperature of 1200 °C proposed in this paper should be sufficient to achieve complete phase transformation of starting HAP/β-TCP mixture into pure β-TCP. However, we have observed this tendency just in the case of CIP samples, if we neglect a few traces of original HAP. All other samples varied in the content of remained HAP, which can be linked to the different shaping methods employed and their corresponding parameters, and thus their influence on green body microstructure.

We have to admit that our study faces certain limitations and opens new questions. First, only one starting powder composition was used (one Ca/P ratio), but diverse starting mixtures can be affected differently by the green body microstructure during sintering. The second opened question is the green body microstructure's impact on the final phase composition when varying the sintering temperature or heating rates. Anyhow, we can state that the green body microstructure is one of the key parameters determining the phase composition of calcium phosphate ceramics after sintering, and it can be influenced significantly by the freeze-casting technique and its parameters.

5. Conclusions

Samples with different microstructures and wide range of porosities were successfully prepared by several techniques, freeze-casting followed by freeze-drying or air-drying, slip-casting and cold isostatic

pressing. The impact of used shaping method on the green body and sintered density, pore distribution, and final phase composition was observed. Mercury porosimetry results (which correlated with SEM micrographs) revealed differences in the porosity. Bimodal pore size distribution was obtained in all freeze-cast + freeze-dried samples, while unimodal distribution was obtained in all freeze-cast + air-dried samples, and conventionally prepared samples.

The sintering behaviour of samples, in which preparation a freezing step was involved, differed from the conventionally prepared ones. The beginning of the densification was shifted about 50 °C to higher temperatures (870 °C vs. 920 °C). A phase transformation of HAP into β-TCP was observed already during the calcination at 800 °C. The residual HAP content in the sintered samples (1200 °C/120 min) was increasing with the higher porosity, as well as the pore size. This trend was observed for both, samples with a unimodal and bimodal pore size distribution. The content of residual HAP in the sintered samples varied for 4%–30% for samples with unimodal pore size distribution and from 7% to 16% for samples with bimodal distribution.

The question raised in the title 'why freeze-casting brings different phase composition of calcium phosphates' could be answered: the freezing rate applied during the freeze-casting has an influence on the resulting porosity and phase composition regardless of whether freeze-drying or air-drying was used afterward.

Declaration of competing interest

The authors declare that they have no known competing financial interests or personal relationships that could have appeared to influence the work reported in this paper.

Acknowledgements

CzechNanoLab project LM2018110 funded by MEYS CR is gratefully acknowledged for the financial support of the measurements at CEITEC Nano Research Infrastructure. The authors also gratefully acknowledge the funding provided by the Czech Ministry of Education under grant LTT18013 (Inter-Transfer). The authors also wish to express their gratitude to JCMM association with ORION project (ORION has received funding from the European Union's Horizon 2020 research and innovation programme under grant agreement Nº 741527), and Brno PhD Talent project, which provides financial support to the first author.

References

[1] María Vallet-Regí, J.Salinas Antonio, Ceramics as bone repair materials, in: Bone Repair Biomaterials 2019, Elsevier, 2019, pp. 141–178, https://doi.org/10.1016/B978-0-08-102451-5.00006-8, 9780081024515.

[2] Nathan W. Kucko, Herber Ralf-Peter, C.G. Leeuwenburgh Sander, John A. Jansen, Calcium phosphate bioceramics and cements, in: Principles of Regenerative Medicine 2019, Elsevier, 2019, pp. 591–611, https://doi.org/10.1016/B978-0-12-809880-6.00034-5, 9780128098806.

[3] Jiwoon Jeong, Kim Jung Hun, Shim Jung Hee, S. Hwang Nathaniel, Heo Chan Yeong, Bioactive calcium phosphate materials and applications in bone regeneration, Biomater. Res. 23 (1) (2019) 1–11, https://doi.org/10.1186/s40824-018-0149-3. ISSN 2055-7124.

[4] Aleksandra Szcześ, Hołysz Lucyna, Chibowski Emil, Synthesis of hydroxyapatite for biomedical applications, Adv. Colloid Interface Sci. 249 (2017) 321–330, https://doi.org/10.1016/j.cis.2017.04.007. ISSN 00018686.

[5] R.G. Carrodeguas, S. De Aza, A-Tricalcium phosphate: synthesis, properties and biomedical applications, Acta Biomater. 7 (10) (2011) 3536–3546, https://doi.org/10.1016/j.actbio.2011.06.019. ISSN 17427061.

[6] I. Manjubala, T.P. Sastry A, R.V. Suresh Kumar, Bone in-growth induced by biphasic calcium phosphate ceramic in femoral defect of dogs, J. Biomater. Appl. 19 (4) (2016) 341–360, https://doi.org/10.1177/0885328205048633. ISSN 0885-3282.

[7] E. Champion, Sintering of calcium phosphate bioceramics, Acta Biomater. 9 (4) (2013) 5855–5875, https://doi.org/10.1016/j.actbio.2012.11.029. ISSN 17427061.

[8] Eliaz, Noam A Noah Metoki, Calcium phosphate bioceramics: a review of their history, structure, properties, coating technologies and biomedical applications, Materials 10 (4) (2017), https://doi.org/10.3390/ma10040334. ISSN 1996-1944.

[9] Kiyoshi Itatani, Nishioka Toshio, Seike Satoru, F. Scott Howell, Akira Kishioka, A. Makio Kinoshita, Sinterability of beta-calcium orthophosphate powder prepared by spray-pyrolysis, J. Am. Ceram. Soc. 77 (3) (1994) 801–805, https://doi.org/10.1111/j.1151-2916.1994.tb05368.x. ISSN 0002-7820.

[10] S. Ramesh, C.Y. Tan, S.B. Bhaduri, W.D. Teng, A.I. Sopyan, Densification behaviour of nanocrystalline hydroxyapatite bioceramics, J. Mater. Process. Technol. 206 (1–3) (2008) 221–230, https://doi.org/10.1016/j.jmatprotec.2007.12.027. ISSN 09240136.

[11] Sylvain Deville, Ice-templating, freeze casting: beyond materials processing, J. Mater. Res. 28 (17) (2013) 2202–2219, https://doi.org/10.1557/jmr.2013.105. ISSN 0884-2914.

[12] Sylvain Deville, Freeze-casting of porous biomaterials: structure, properties and opportunities, Materials 3 (3) (2010) 1913–1927, https://doi.org/10.3390/ma3031913. ISSN 1996-1944. Available at, http://www.mdpi.com/1996-1944/3/3/1913.

[13] Sylvain Deville, Saiz Eduardo, P. Antoni, TOMSIA. Freeze casting of hydroxyapatite scaffolds for bone tissue engineering, Biomaterials 27 (32) (2006) 5480–5489, https://doi.org/10.1016/j.biomaterials.2006.06.028. ISSN 01429612.

[14] S. Deville, Freeze-casting of porous ceramics: a review of current achievements and issues, Adv. Eng. Mater. 10 (3) (2008) 155–169, https://doi.org/10.1002/adem.200700270. ISSN 14381656.

[15] Ulrike G.K. Wegst, Schecter Matthew, E. Amalie, Donius, M. Philipp, Hunger, Biomaterials by freeze casting, Phil. Trans. Math. Phys. Eng. Sci. 368 (1917) (2010) 2099–2121, https://doi.org/10.1098/rsta.2010.0014. ISSN 1364-503X.

[16] Seifert, Annika, Jürgen Groll, Jan Weichhold, Anne V.Boehm, Frank A.Müller and Uwe Gbureck. Phase conversion of ice-templated α-tricalcium phosphate scaffolds into low-temperature calcium phosphates with anisotropic open porosity. Adv. Eng. Mater.. ISSN 1438-1656. DOI: 10.1002/adem.202001417.

[17] Zheng-Quan Jia, Guo Zuo-Xing, Fei Chen, Li Jing-Juan, Zhao Lei, Li Zhang, Microstructure, phase compositions and in vitro evaluation of freeze casting hydroxyapatite-silica scaffolds, Ceram. Int. 44 (4) (2018) 3636–3643, https://doi.org/10.1016/j.ceramint.2017.11.114. ISSN 02728842.

[18] E. Meurice, F. Bouchart, J.C. Hornez, et al., Osteoblastic cells colonization inside beta-TCP macroporous structures obtained by ice-templating, J. Eur. Ceram. Soc. 36 (12) (2016) 2895–2901, https://doi.org/10.1016/j.jeurceramsoc.2015.10.030. ISSN 09552219.

[19] Hyun Lee, Jang Tae-Sik, Song Juha, Kim Hyoun-Ee, Jung Hyun-Do, The production of porous hydroxyapatite scaffolds with graded porosity by sequential freeze-casting, Materials 10 (4) (2017), https://doi.org/10.3390/ma10040367. ISSN 1996-1944.

[20] J. Roleček, L. Pejchalová, F.J. Martínez-Vázquez, P. Miranda González A, D. Salamon, Bioceramic scaffolds fabrication: indirect 3D printing combined with ice-templating vs. robocasting, J. Eur. Ceram. Soc. 39 (4) (2019) 1595–1602, https://doi.org/10.1016/j.jeurceramsoc.2018.12.006. ISSN 09552219.

[21] EN 13383-1, Fine Ceramics (Advanced Ceramics, Advanced Technical Ceramics): Microstructural Characterization - Part 1: Determination of Grain Size and Size Distribution, International Organization for Standardization, 2012.

[22] EN 623-2, Advanced Technical Ceramics; Monolithic Ceramics: General and Textural Properties; Determination of Density and Porosity, International Organization for Standardization, 1993.

[23] Jeffrey M. Toth, M.Hirthe Walter, G.Hubbard William, A.Brantley William, A. Kenneth, L. Lynch, Determination of the ratio of HA/TCP mixtures by x-ray diffraction, J. Appl. Biomater. 2 (1) (1991) 37–40, https://doi.org/10.1002/jab.770020106. ISSN 10454861.

[24] K. Maca, V. Pouchly A, A.R. Boccaccini, Sintering densification curve: a practical approach for its construction from dilatometric shrinkage data, Sci. Sinter. 40 (2) (2008) 117–122. ISSN 0350-820X.

[25] S. Deville, Freezing as a path to build complex composites, Science 311 (5760) (2006) 515–518, https://doi.org/10.1126/science.1120937. ISSN 0036-8075.

[26] Jumeng Zheng, Winnubst Louis, Shumin Fang Velianti, A. David Salamon, Manipulation of sintering behaviour by initial freeze pressing an aqueous alumina suspension, Adv. Eng. Mater. 13 (1–2) (2011) 77–81, https://doi.org/10.1002/adem.201000199. ISSN 14381656.

[27] Z. Zyman, J. Weng, X. Liu, X. Li, A.X. Zhang, Phase and structural changes in hydroxyapatite coatings under heat treatment, Biomaterials 15 (2) (1994) 151–155, https://doi.org/10.1016/0142-9612(94)90265-8. ISSN 01429612.

[28] Kuo-Tien Chu, Ou Shih-Fu, Shyuan-Yow Chen, Chiou Shi-Yung, Chou Hsin-Hua, A. Keng-Liang, Ou, Research of phase transformation induced biodegradable properties on hydroxyapatite and tricalcium phosphate based bioceramic, Ceram. Int. 39 (2) (2013) 1455–1462, https://doi.org/10.1016/j.ceramint.2012.07.089. ISSN 02728842.

[29] Shih-Fu Ou, Shi-Yung Chiou, A. Keng-Liang, Ou, Phase transformation on hydroxyapatite decomposition, Ceram. Int. 39 (4) (2013) 3809–3816, https://doi.org/10.1016/j.ceramint.2012.10.221. ISSN 02728842.